Polym. Bull. (2010) 65:181–199
DOI 10.1007/s00289-010-0248-3

ORIGINAL PAPER

Assembly, characterization of Ag nanoparticles in P(AAm-co-NVP)/CS semi-IPN, and swelling of the resulting composite hydrogels

Yan-Ling Luo · Feng Xu · Ya-Shao Chen · Chun-Yang Jia

Received: 19 October 2009 / Revised: 31 December 2009 / Accepted: 5 January 2010 /
Published online: 21 January 2010

Abstract Silver nanoparticles (AgNPs) with controlled size and size distribution were prepared by an in situ chemical reduction route based on a microreactor template composed of poly(acrylamide-co-*N*-vinylpyrrolidone)/chitosan semi-interpenetrating network hydrogels, P(AAm-co-NVP)/CS semi-IPN, in the presence of sodium hypophosphite. The characterization of structures and morphologies of the as-fabricated P(AAm-co-NVP)/CS–Ag nanocomposite hydrogels was conducted on a Fourier transformation infrared spectroscopy (FTIR), scanning electron microscope (SEM), transmission electron microscope (TEM), and UV–vis spectrometer. The effect of various component proportions of the reactants on formation of AgNPs and swelling of the resulting P(AAm-co-NVP)/CS–Ag nanocomposite hydrogels was investigated. The experimental results indicated that the Ag grains were uniformly dispersed within P(AAm-co-NVP)/CS hydrogel networks in a spherical shape, and were stabilized by the semi-IPN structure and a complexation and/or electrostatic interaction between Ag^+ cations and chemical functional groups, such as –OH, $–CONH_2$, $–NH_2$ or –C=O based on the semi-IPN structure reactor templates. The size of the majority of AgNPs ranges from 12 to 25 nm, depending on the three-network templates, the presence of functional groups as well as feed ratios of *N*-vinylpyrrolidone, acrylamide, and chitosan. Thermogravimetric analysis (TGA) provides the stability of the resulting nanocomposite hydrogels. The nanocomposite hydrogels demonstrate reduced swelling in comparison with the P(AAm-co-NVP)/CS ones. The kinetics modeling confirms that transport mechanism of the samples follows anomalous diffusion mode, and the kinetic parameters

Y.-L. Luo (✉) · F. Xu (✉) · Y.-S. Chen · C.-Y. Jia
Key Laboratory of Macromolecular Science of Shaanxi Province, School of Chemistry and Materials Science, Shaanxi Normal University, Xi'an 710062, People's Republic of China
e-mail: luoyanl@snnu.edu.cn

F. Xu
e-mail: fengxu@snnu.edu.cn

vary with the component ratios, and the maximal theoretical water volume S_∞ is well in agreement with the experimental values.

Keywords Nanocomposite hydrogels · Swelling · Non-covalent interactions · Chemical synthesis · Ag nanoparticles · Optical properties

Introduction

In recent years, the exploitation of nano-materials is in the forefront of chemistry, physics, and materials science research, one of the hottest subjects. Size- and shape controllable metal nanoparticles or atom clusters, especially silver particles, have attracted considerable attention due to their peculiar physical and chemical properties [1–7]. Their bulk effect, surface effect and quantum size effect, have endowed them with a vast application foreground in catalysts and antibacterial materials, medication, biological sensors, optical or nonlinear optical, magnetic, superconductive, and electronic devices. A variety of preparation methods of nano-silver powders include thermal decomposition, chemical reduction, biochemical, gas condensation, electrochemical, microwave reduction routes, irradiation, ultrasonication, and actinochemistry means [8–11]. The chemical reduction is the simplest and most effective means, and a large number of reducing agents, e.g., trisodium citrate, ethylenediaminetetraacetate, glycol, and sodium borohydride, are available to deoxidize Ag^+ to Ag nanoparticles (AgNPs). Widespread issues during preparation of AgNPs, however, are the un-stability of the as-formed particles, the irregular shape as well as a wide range of size distribution, and are prone to agglomerate. Consequently, their synthesis or preparation has been being a challenging subject in a nanomaterials science field all the time.

In order to achieve AgNPs with effective antioxidation avoiding collision, a series of measures are proposed and developed, including using polymers, biomacromolecules, latex particles, mesoporous inorganic materials, hyperbranched polymers, dendrimers, microporous gels or hydrogels and colloid systems, and so on [5–7, 12–14]. Hydrogel or macroscopic gels as promising templates or nanopots have been used to prepare nanoparticles, thus having brought a concept for newer composite/hybrid materials [2, 15]. The in situ synthesis of NPs in microbeads, such as ion exchange resins, latex spheres, or microgels has a 2-fold advantage: the use of polymer spheres as the microreactors and the production of a material with structural hierarchy [16]. Their unique three dimensional networks, as a template of nanoparticles assembly, may impose confinement and guiding roles on topologies and size of nanoparticles, and thus reserve to grew and stabilize the nanoparticles [17]. At the same time, the size and size distribution can be mediated by cross-linkers, components, and compositional proportion [2, 4, 6, 18, 19]. The mesh size, non-covalent interactions between metal ions and –OH, $–CONH_2$, $–NH_2$, or –C=O functional groups, steric hindrance as well as reducing ability may have important impact on the nucleation, particle growth and collision, which is in turn responsible for the fabrication and stabilization of the size- and shape-controllable metal nanoparticles. Since sodium hypophosphite has a strong reducing ability, a protectant

should be introduced to retard the reduction rate to obtain nanoparticles. Poly(*N*-vinylpyrrolidone) (PVP) and chitosan (CS) are good protectants or dispersants preparing nanoparticles, and play an important part in the controllable production and stabilization of nanoparticles with definite size. Moreover, they both can reduce Ag^+ ions to some extent, and promote the nucleation of AgNPs [20, 21]. Poly(acrylamide) (PAAm) hydrogels are also employed to prepare highly distributed AgNPs and to control particle number [4, 15]. Therefore, PMAA, PVP, and CS as typical polymers used to assemble nanoparticles will make sense. Moreover, such supramolecular interaction as complexation and/or electrostatic interaction between Ag^+ cations and chemical functional groups, such as –OH, $–CONH_2$, $–NH_2$, or –C=O will allow us to well-understand fundamental assembly principles of metal NPs.

The resulting metal nanoparticles/polymer hybrid hydrogel materials can potentially be applied in catalysis, sensors, actuators, and microfluidic devices as well as separation technology [2], reflecting the AgNP properties. Furthermore, these nanocomposite systems are highly suitable for the pharmaceutical and biomedical applications due to their good bio-compatibility over biological molecules, cells, tissues, etc. [19, 22–24]. K. Vimala et al. studied swelling of AgNP/PAAm hydrogels, etc. for bioapplications [15, 19]. AgNPs are generally considered as environmentally friendly antibacterial materials. The AgNP/PVP composite as a bactericide is applied in complicated cases of infected burns and purulent wounds [2]. However, their electronic properties recently were reported to be used in biosensors and drug delivery applications as well as drug carriers for biomolecules such as enzymes [19, 22]. In practice, gold nanoparticles are the most commonly used nanoparticles for diagnostics and drug delivery. The unique chemical properties of colloidal gold make it a promising targeted delivery approach for drugs or gene specific cells. Gold and silica composite nanoparticles have been investigated as nanobullets for cancer [24]. These preliminary research results have prompted us to draw a new idea in which the combination of PAAm, PVP, and CS with more relevance for pharmaceutical and biomedical applications are selected as matrix materials of semi-IPN hydrogels and employed to assemble AgNPs. An important tool in the design of targeted delivery vehicles is a nanoparticle platform, in which the physicochemical parameters can be independently controlled for in vivo evaluation. We expect to make progress in this application area.

In consideration of the mentioned concerns, the objective of this contribution is to synthesize a type of semi-interpenetrating networks (semi-IPN) hydrogels as a microreactor template based on AAm, NVP, and CS with hydrophilic nature for anchoring/reduction of metal ions and stabilization, which would be better choice to cook AgNPs in the interior of hydrogel networks. While the nucleation, particle growth, and collision of AgNPs can be mediated by means of a non-covalent interaction between Ag^+ cations and chemically functional groups inside P(AAm-co-NVP)/CS hydrogel networks, including a coordinate bond (forming a ligand complex) and/or an electrostatic action. Consequently, this study features a new production technology for metal nanoparticles manipulated by multicomponent polymeric complexes that are candidates for delivery vehicles of biological molecules, such as proteins and drugs. It is demonstrated that the hydrogel network structure determines the size and shape of the nanoparticles. These particles are

more stable in the gel networks compared to other reduction methods. Therefore, highly stable and uniformly distributed AgNPs with predetermined dimensions and size-dependent properties have been achieved by a very delicate balance between the reaction conditions, the composition and the structure of microgel templates, and the concentration of AgNPs in the hydrogels. To the best of our knowledge, this is the first comprehensive study of the in situ synthesis technology of AgNPs in hydrogel templates manipulated by multicomponent polymeric complexes that are candidates for delivery vehicles of biological molecules, such as proteins and drugs.

Compared with other polymer templates like dendrimers, block copolymer micelles, and star block copolymers, polymer microgels have the advantages of simple synthesis and easy functionalization [16]. However, the main advantages originating from their network structure are: each void can be used for AgNPs nucleation and growth, microgels undergo volume transitions in response to external stimuli, and functional species other than AgNPs, e.g., small protein or drug molecules, can be incorporated and then released from the interior of microgels. It is expected that this study, a production technology of AgNPs based on the semi-IPN structure reactor templates, combined with complexation and/or electrostatic interaction between Ag^+ cations and chemical functional groups, will have some science significance in preparation of metal NPs and applications in drug carriers, sterilization, or medication materials.

Materials and methods

Materials

The acrylamide (AAm), analytical grade (A.G.), was supplied by the Xi'an Chemical Reagent Factory, China. *N*-vinyl pyrrolidone (NVP, A.G.) was supplied by the Sigma-Aldrich Chemie GmbH, Germany. Ammonium persulphate (APS, A.G.), as a free-radical initiator, supplied by the Xi'an Chemical Reagent Factory, was recrystallized before use. *N*,*N*-methylenebisacrylamide (NNMBA, A.G.), used as a cross-linker, was purchased from the Tianjin Kermol Chemical Regent Developing Center. *N*,*N*,*N*′,*N*′-tetramethylethylenediamine (TEMED, A.G.) as an accelerant was obtained from the Beijing Dingguo Biotechnologies Corp. Ltd., used as received. The chitosan (CS), provided by the Wolsen Corp., Japan, served as both an interpenetrating component and a stabilizer, with Da of ca. 1.0×10^5. $AgNO_3$ (A.G.) was supplied by the Shanghai Institute of Fine Chemicals and Industrial Materials. Sodium hypophosphite ($Na_2H_2PO_2 \cdot H_2O$, A.G.), as a reducer, was purchased by the Shenyang Reagent Factory No. 3. The acetic acid (A.G.) was from the Xi'an Chemical Reagent Manufactory. All chemicals were used without further purification.

Preparation procedures

Synthesis of P(AAm-co-NVP)/CS semi-IPN hydrogels

P(AAm-co-NVP)/CS semi-IPN hydrogels were synthesized using a simple free radical polymerization approach. Various concentrations of the CS in terms of

Table 1 Compositions and charge ratios of P(AAm-co-NVP)/CS semi-IPN hydrogels

Samples	A	B	C	D	E	F	H	I	G
NVP (mg)	1000	1000	1000	600	600	600	200	200	200
AAm (mg)	1000	1000	1000	1400	1400	1400	1800	1800	1800
CS (mg)	20	40	100	20	40	100	20	40	100

* Unless otherwise stated, all the samples possess the compositions and charge ratios of this table hereinafter. 2 wt% CH_3COOH and 1 wt% APS both are 5.0 mL in all experimentations. The amount of the crosslinker NNMBA accounts for 1 wt% of the total weight of NVP and AAm monomers

Table 1 was fully dissolved in a 5 mL 2 wt% acetic acid solution, and then NVP and AAm monomers were plunged into the CS–acetic acid solution according to corresponding charge ratios in Table 1. After the stirring proceeded for about 10 min, 5 mL 0.2 mol L^{-1} APS solution and 0.02 g 1 wt% (the total weight of the monomers) NNMBA were introduced into the reaction mixture under rapid stirring at 60 °C for another 5 h. The products were immersed for 7 days and flushed with deionized water to remove residues of the unreacted monomers and various reagents. The resulting hydrogels were dried in a vacuum oven at 35 °C until constant weight.

Fabrication of AgNPs in P(AAm-co-NVP)/CS semi-IPN networks

The assembly of AgNPs in the P(AAm-co-NVP)/CS semi-IPN hydrogel networks has been performed in the following steps. A certain amount of dry hydrogels were equilibrated with 30 mL high-pure water for 3 days. At this time, most of the silver ions are exchanged from solution into hydrogel networks by anchoring through –C=O, $–CONH_2$, $–NH_2$, or –OH groups of hydrogel chains and rest of metal ions occupied free-network spaces of hydrogel networks. Next, the swollen hrdrogels were transferred into a beaker containing 30 mL of a 0.5 mol L^{-1} $AgNO_3$ aqueous solution to diffuse for 24 h. These hydrogels loaded with sliver salts were subsequently immersed in 30 mL of a 0.5 mol L^{-1} $Na_2H_2PO_2$ aqueous solution to induce Ag^+ ions into AgNPs. After the reduction reaction was carried out at room temperature (25 °C) for 3 h, the samples were dried at 35 °C in a vacuum oven until constant weight.

Determination and characterization

The structural characterization of P(AAm-co-NVP)/CS and P(AAm-co-NVP)/CS–Ag samples was carried out on an EQUINX55 Fourier transform infrared spectroscope (FT-IR) manufactured by the Blucker Corp, Germany, using the method of the potassium bromide tableting. The morphological characterization of the samples was conducted on a Quanta 200 SEM produced by the Philips-FEI Corp, Holland, with an operating voltage of 20 kV and a current of 30 mA. Transmission electron microscope (TEM) observations were performed on a Hitachi H-600 electron microscope at an accelerating voltage of 75 kV to obtain

information of the size, shape, and dispersity of the silver nanoparticles in the semi-IPN matrix. Before observed, a specimen was prepared by dispersing the nanocomposite samples in an ethanol solution, and then spreading a small drop of the solution on a carbon-coated copper grid and allowing the drop to dry completely in air. UV–visible spectra were recorded on a TU-1901 spectrometer (Purkinje General Instrument, Beijing, China). The thermal stabilities of the resulting nanocomposites were evaluated on a Q1000DSC + LNCS + FACS Q600SDT thermoanalyzer system (TGA, the TA Corp. USA) at a heating rate of 10 °C min^{-1} under N_2 atmosphere (flow rate, 40 mL min^{-1}).

In order to understand the swelling of the as-assembled P(AAm-co-NVP)/CS–Ag nanocomposite hydrogels, the dried hydrogels were immersed in an excess amount of deionized water at room temperature until swelling equilibrium was attained. The wet weight of the sample (W_s) at time t was determined after removing the surface water by blotting with filter paper, and the equilibrium water content was designated (W_e). The dry weight (W_d) was recorded after drying the sample in a vacuum oven at room temperature for 3 days. The swelling ratio (R) and equilibrium degree of swelling (R_e) of the samples were calculated from the following equations [25–27]:

$$R = (W_s - W_d)/W_d \quad (1)$$

$$R_e = (W_e - W_d)/W_d. \quad (2)$$

Results and discussion

Hydrogels as a template for synthesis of metal nanoparticles are involved in loading and reducing of metal salts, for instance, Ag^+ ions. In general, the ion exchange process between Ag^+ ions present in the external immersion medium and H^+ ions within the interior of the gel phase may act as a main driving force for entrance of silver ions into the network for hydrogels containing poly(acrylic acid) homologs [28, 29]. Due to a strong electrostatic interaction, the Ag^+ ions are anchored by the COO^- groups. However, in poly(2-hydroxyethyl methacrylate-poly(ethylene glycol) methyl ether methacrylate) (PHP) hydrogel, the Ag^+ ions diffuse randomly in the gel network due to absence of binding [19], and hence the reduced AgNPs form aggregates. In this study, owing to the existence of the complexation and/or electrostatic interaction between Ag^+ cations and chemical functional groups, such as –OH, $–CONH_2$, $–NH_2$, or –C=O on polymer chains, an ion exchange process mainly drives Ag^+ ions into the hydrogel networks. Upon adding the fully swollen hydrogels to the aqueous solution of Ag^+ salt, the Ag^+ ions get absorbed or anchored by the polymer network via an ion exchange process of the above functional groups, or only by entrapment of Ag^+ ions in the free space existing between the cross-linked gel networks [15, 28, 30]. The reduced AgNPs are therefore stabilized.

The existing free spaces between cross-linked hydrogel networks in the swollen state also act as nanoreactors or templates for nanoparticle nucleation and growth and provide long-term stability. Many researches have reported influence of dimension of free spaces resulting from crosslinking densities on size or content,

and morphologies of AgNPs within the gel [2, 28–30]. Highly denser hydrogel networks (altering concentration, and kinds of crosslinkers as well as the combination of different crosslinkers) would help to obtain lower sized AgNPs, since less free space in the hydrogel networks favors to establish more intra–inter molecular attractions between gel networks, while lower crosslinked gel networks provide enough free space to grow greater nano-sized particles [2, 29]. Therefore, the crosslink density appears to be a key factor in stabilizing and regulating the shape and size of nanoparticles. Based on the description, we have focused on the nature of monomers or the overall functionality of semi-IPN polymer chains with various component ratios under the identical degree of cross-links or the concentration of cross-linkers.

FT-IR analysis

To verify the structural information about polymer hydrogels, FT-IR analysis is carried out, as displayed in Fig. 1. The AAm monomer (Fig. 1a) shows characteristic absorption peaks at about 3,361 and 3,190 cm^{-1} corresponding to the asymmetric and symmetrical stretch vibration bands of $–NH_2$ groups, at 1,677 and 1,612 cm^{-1} assigned to the stretching vibration of carbonyl groups (C=O) and the N–H bend vibration of amide groups or C=C absorption [31], at 1,433 and 1,348 cm^{-1} due to =C–H vibration of AAm units. The NVP monomer (Fig. 1b) shows characteristic absorption bands at 2,360 cm^{-1} attributable to $–NR_2$ peak, at 1,391 cm^{-1} ascribed to =C–H, at 1,088 cm^{-1} related to C–C backbone (skeletal vibration), and at 1,024 cm^{-1} related to C–C bands on the NVP cyclic structure. The peaks at 1650, 1432, 1260, and 1167 cm^{-1} belong to C=O stretching of cyclic amide or C=C of NVP, C–H stretch or ($–CH_2–$) C–H twist, C–N stretch, and $–CH_2–$ rocking, respectively [32]. The CS spectrum (Fig. 1c) presents characteristic peaks at 3,454 cm^{-1} assigned to stretching vibration of $–NH_2$ and –OH groups, at 2,925 cm^{-1} due to –C–H stretch, at 1,700 cm^{-1} associated with $–NH_2$ deformation

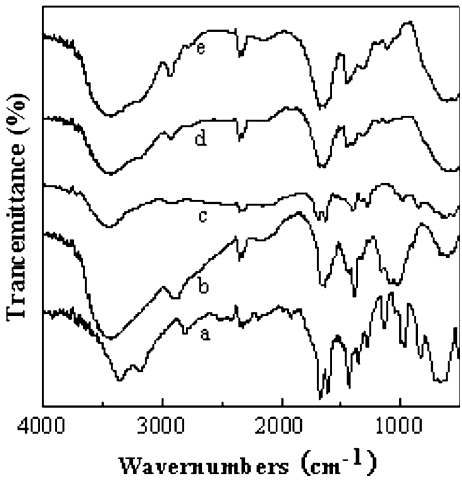

Fig. 1 FTIR spectra of (*a*) AAm, (*b*) NVP, (*c*) CS, (*d*) P(AAm-co-NVP)/CS hydrogel, and (*e*) P(AAm-co-NVP)/CS–Ag nanocomposite hydrogel

vibration, at 1632, 1276, and 1396 cm^{-1} belonging to –N–H bend [26, 33], at 1060 cm^{-1} related to the –C–O– or bridge-O stretch vibration, and at 600–640 cm^{-1} reflecting the pyranoside ring stretching vibration in CS skeleton [34, 35]. In Fig. 1d, the existence of major characteristic peaks proves the formation of the expected P(AAm-co-NVP)/CS hydrogel moiety. The occurrence of a new absorption peak at 2,928 cm^{-1} ascribed to the –C–H stretching band further indicates that the monomers are successfully polymerized and crosslinked in the presence of CS by breaking the C=C bond [35]. The slight shift of absorption peaks from 1653 to 1684 cm^{-1} is most probably due to influence of polysaccharide on amide groups of PVP chains [36, 37]. The FT-IR spectra of the resulting nanocomposites (Fig. 1e) present absorption intensity changes of –C=O, $–NH_2$, or –OH groups due to the introduction of AgNPs and AgNPs interaction with hydrogel networks. Therefore, we infer that AgNPs are assembled in free-network spaces of hydrogels or anchored on the surface of hydrogels.

Optical properties

The formation and stability of the reduced AgNPs in the colloidal solution with the hydrogel networks as nanoreactor templates are further monitored using UV–vis spectral analysis, as depicted in Fig. 2. All the samples exhibit an absorption band at around 395–410 nm, which is a typical plasmon band, suggesting the formation of AgNPs with small size [20, 38]. Namely, the absorption of the light is produced by certain size of precious metal nanoparticles through a continuous oscillation resulting from an interaction between the valence band electrons and the electromagnetic field, or surface plasma resonance (SPR) [20], which is an expression of a small particle

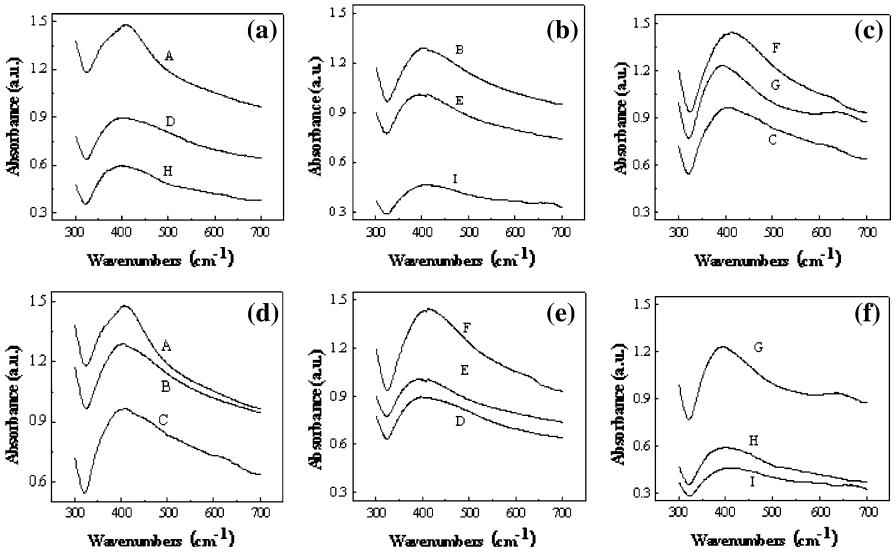

Fig. 2 UV–vis spectra of P(AAm-co-NVP)/CS–Ag nanocomposite hydrogels assembled using the hydrogel networks as templates

size effect and does not exist in the bulk materials. From Fig. 2a–c, we notice that the intensity of the SPR absorption peaks is weakened and the full width at half-maximum (FWHM) is enlarged with reducing the charge ratios of NVP to AAm, reflecting decreased AgNP number, and broadened particle size distribution. Meanwhile, the center of the absorption peaks transits slight blue shift, corresponding to a drop in particle sizes. It is quite evident that the charge ratios and some interaction between the three components and Ag^+ ions may have dominant effects on the optical traits, which may alter the number of nucleation, the protected and confined function, and further be responsible for the grain size, distribution, and number of the formed AgNPs [38]. Actually, these components operate as a controller of nucleation as well as a stabilizer. These results are consistent with that reported in literatures [39–45], which describe the binding character of colloidal Ag onto secondary amine, hydroxyl groups. Ag^+ ions are anchored onto the polymer surfaces via electrostatic (i.e., ion–dipole) or coordination interactions (i.e., N–Ag^+ or O–Ag^+ metal–ligand complex) [39–42]. The as-reduced AgNPs are then surrounded by the polymer molecules. Such a steric hindrance effect can not only control the reaction rate but also restrain AgNPs from the formation of large particles due to a collision, therefore hindering the aggregation of AgNPs [40]. The complexation of silver by chitosan via the Ag–O bond, and the interaction between PVP and AgNPs were confirmed by XPS measurement [42–45] as well as FTIR results in our study. In addition, PVP molecules may reduce Ag^+ ions, promoting the nucleation of AgNPs, controlling the size of AgNPs, supplying the dispersion stabilization and preventing from aggregation [40]. It is due to the strong coordination localization that Ag^+ ions are immobilized in free-network spaces of hydrogels or on the surface of these polymer networks [41]. All these help in modulating and controlling the size of the nanoparticles and supplying better stability. In Fig. 2c, the reason why the absorption intensity for sample C is decreased may have relation to a high CS concentration at a lower MAA ratio to NVP. Further, we find in Fig. 2d that the intensity of the absorption peaks decreases, and the FWHM and particle size distribution are broadened with increasing the content of CS, whereas Fig. 2e and f give opposite results, which may suggest a correlation with increased concentrations of AAm. In addition, a slight blue shift with the CS concentrations in Fig. 2d and e means a reduction in particle size. The two distinctly opposed results once again illuminate that the assembly of AgNPs can be accomplished by varying the component ratios of NVP, AAm, and CS at the same time, based on their respective interaction with Ag^+ ions with the hydrogel networks as templates.

TEM and SEM observations

In order to intuitively observe the morphologies of the assembled AgNPs, TEM micrographs of P(AAm-co-NVP)/CS–Ag nanocomposite hydrogels consisting of various mass ratios of AAm, NVP, and CS components are taken, as shown in Fig. 3. The size and the size distribution of the Ag nanoparticles may be analyzed by dynamic light scattering (DLS). They, however, are not able to be readily determined in this study in that Ag nanoparticles are assembled and immobilized or

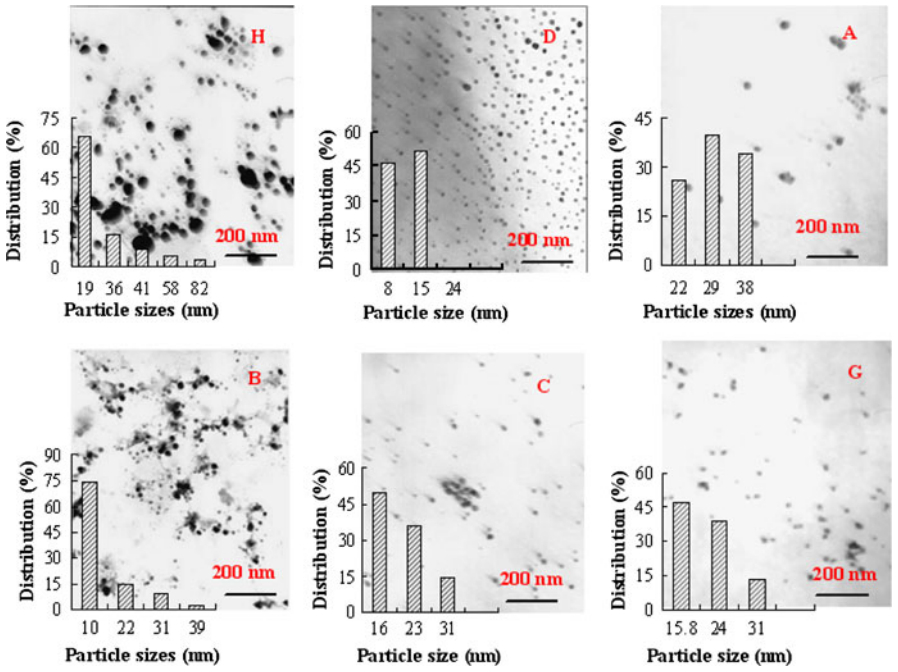

Fig. 3 TEM micrograms and corresponding particle size histograms of various P(AAm-co-NVP)/CS–Ag nanocomposite hydrogels

attached inside the P(AAm-co-NVP)/CS semi-IPN and non-particle P(AAm-co-NVP)/CS–Ag nanocomposite gels are formed. Therefore, we evaluated the size distribution on the basis of statistical analysis on TEM results. In general, at least 150–300 particles for each sample are typically measured [46]. In this study, we first obtain nuclei sizes of 200 Ag particles, and further determine the average size of particles and their distribution. The mean particle size is estimated according to the following formula:

$$D_n = \sum n_i D_i \Big/ \sum n_i \tag{3}$$

where D_n represents number average particle diameters of the as-prepared Ag nanoparticles, and n_i is the number of the nanoparticles with diameter D_i. It is worthy to note that the number of particles is not limited to the given images in Fig. 3, which is only a representative.

It is evident that the Ag particles are spherical in shape. The nanoparticles are homogeneously dispersed in the semi-IPN templates, and the size of the majority of AgNPs is estimated in the range of 8–31 nm, and the mean size is about 14, 21, 12, and 22 nm in order of samples B, C, D, and G. Most of the AgNPs with particle size of approximate 8–15 or 16–24 nm are predominantly grown and assembled in a preferred distribution except that several large grains (the mean dimension: 28 nm) and a relatively broad size distribution occur in sample H. Sample A possess a relatively large size and the mean size is 30 nm. No conglomeration of Ag colloidal

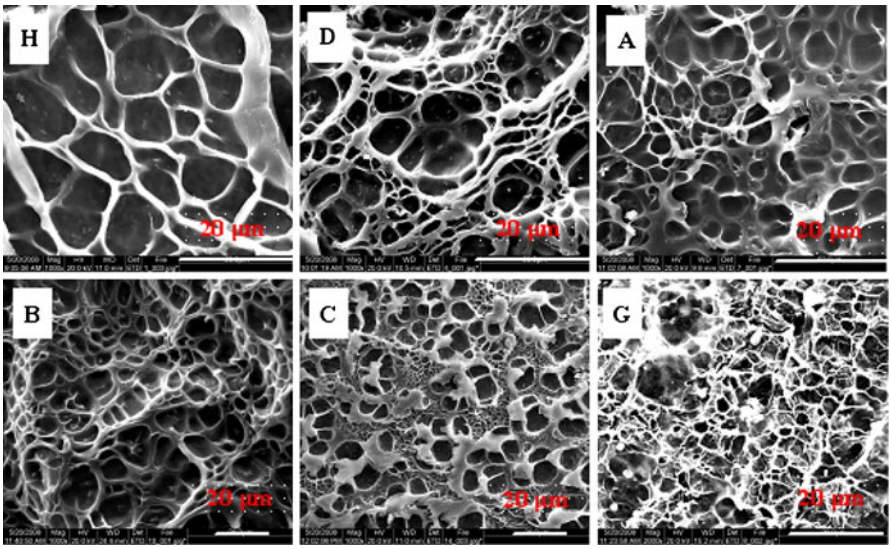

Fig. 4 SEM images of P(AAm-co-NVP)/CS hydrogel networks with various component ratios as templates

particles exists and Ag particles are separated into single ones, and are well-dispersed and stabilized in the semi-IPN matrix. The probable explanations are described in the foregoing UV–vis analysis. In addition, it is reported that high viscosity of the system can prevents the movement, growth, and aggregation of nanosized metal colloidal particles [10]. At the same time, PAAm and PVP are easily attached to the surface of the Ag nanocrystal due to existence of the O=C–N group, which lowers the surface free energy of nanosized metal, stabilizes it, and restrains its growth and aggregation.

In order to evaluate the effect of P(AAm-co-NVP)/CS networks as a nanoreactor template on assembly of AgNPs, SEM observations are performed after the samples are treated by a lyophilization process. Before observations, the lyophilized samples were fractured and the cross-sections were coated with gold films over 80 s in sputter coater. Figure 4 shows SEM images of P(AAm-co-NVP)/CS hydrogels at various mass ratios of AAm, NVP, and CS, respectively. It is quite evident that all the P(AAm-co-NVP)/CS hydrogels display analogous typologies of micropores due to equivalent quantity of crosslinker, which are the basis of nanoreactor templates. It is, however, worthy to note that the sample H with the lowest CS content and highest component ratio of AAm to NVP yields a larger average porous size than samples D and A, and from A to B to C, the pore size is slightly different with increasing CS concentrations, suggesting that the component ratios may have somewhat impact on the morphologies of the hydrogels. In other words, mesh sizes of the hydrogels can be trimmed by adjusting the charge ratios in the same concentration of crosslinkers.

In general, the particle size of AgNPs can be determined or tailored by varying the initial Ag^{+} concentration and the crosslinking densities of hydrogel networks

[28, 29, 42]. In this study, AgNPs are assembled and grown based on the above nanoreactor templates. It can be supposed that it is the confinement and guiding role of gels that guarantees the homogeneous, spherical and nanoleveled Ag particles. Tiny variations in the mesh size of the hydrogels and steric hindrance, reducing ability as well as non-covalent interactions between Ag^+ ions and functional groups originating from different feed ratios of the three components [15] also influence the nucleation and immobilization of Ag particles, giving rise to a slight difference in particle size. The dependence of size control capacity on functional groups has been described in the foregoing UV–vis analysis. Therefore, it may be believed that either Ag particles with larger size or broader distribution for sample H than other ones, or highly stable and uniformly distributed AgNPs with predetermined small dimensions of Ag grains and size-dependent properties, appears to be achieved by a very delicate balance between the reaction conditions, the composition and the structure of microgel templates, and the concentration of AgNPs in the hydrogels. Namely, this study features a new production technology for metal nanoparticles manipulated by multicomponent polymeric complexes. The size, shape, and distribution of AgNPs can effectively be manipulated and controlled by the polymeric hydrogel network structures in the presence of various component ratios [47, 48]. In our opinion, the designed semi-IPN hydrogels are excellent nanoreactors for the synthesis of metal and semiconducting nanoparticles.

Reproducibility and stability

In order to validate the reproducibility of the as-prepared Ag nanoparticles, the sample D as a typical example was valued at the present experimental condition, as given in Table 2. Table 2 indicates high batch-to-batch reproducibility of the diameters of the AgNPs. The relative standard deviation (R.S.D.) is approximately 3.2% for six independent assays, showing a small dispersive degree of grain diameter distributions and an acceptable repeatability. Hence, monodispersed AgNPs can be obtained. This finding implies that the present route will be useful for the mass-production of AgNPs.

The thermal stability of the resulting P(AAm-co-NVP)/CS–Ag nanocomposites was examined by TGA, as illustrated in Fig. 5. The nanocomposite exhibits more excellent thermal stability than its hydrogel template. After three degradation stages, the composite produces about 17% weight loss below 400 °C, <37% loss of the hydrogel template, due to the presence of AgNPs formation inside the nanocomposite hydrogel network. This further supports the interaction between

Table 2 Repeatability of the mean diameters and size distributions of the as-prepared AgNPs

Reaction run	1	2	3	4	5	6
Particle diameter (nm)	12	11.6	11	12.1	11.4	11.5
Standard deviation (nm)	0.38	0.37	0.35	0.39	0.36	0.37

Reaction conditions correspond to sample D

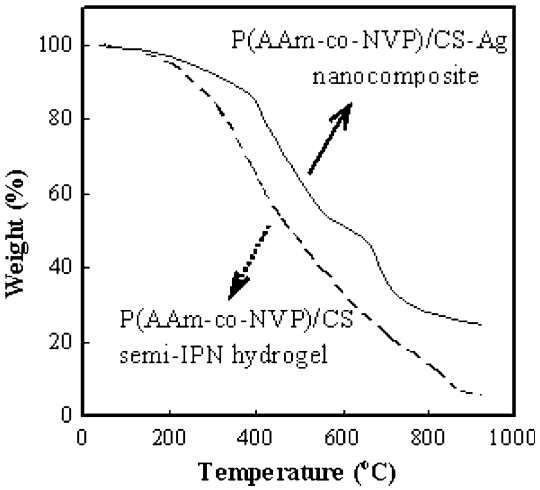

Fig. 5 TGA curves of P(AAm-co-NVP)/CS semi-IPN hydrogel and P(AAm-co-NVP)/CS–Ag nanocomposite material

chemical groups and Ag^+ ions, and thus improving the thermal stability of the resulting product.

Swelling behavior and kinetic analysis

P(AAm-co-NVP)/CS–Ag nanocomposite hydrogels exploited in this study not only have created the possibility of preparing AgNPs with various sizes but also have influenced swelling modes of the gels. Figure 6 compares equilibrium swelling of P(AAm-co-NVP)/CS with P(AAm-co-NVP)/CS–Ag samples having different feed ratios. It is clear that the nanocomposite hydrogels is found to produce lower equilibrium swelling ratios than the control samples, P(AAm-co-NVP)/CS hydrogels. The reason may be related to the fact that when the P(AAm-co-NVP)/CS–Ag nanocomposite hydrogels assembled with AgNPs are immersed in water, the gel networks are fleetly swelled. In this case, the micropores are more easily walled up, reducing the water volume. Sample H containing more AgNPs has the lowest R_e value. It is worth noting that the fluctuation of R_e values for the bare hydrogels in Fig. 6 depends on different hydrogel systems (A, B, C, D, and H), which consist of AAm, NVP, and CS with various feed ratios. A higher R_e value for sample H than other ones appears to correspond to its pore size, which more or less suggests that the swelling seems to be related to the pore size of the gels [49, 50]. Swelling kinetic data in Fig. 7 denote that these prepared samples exhibit typical swelling features analogous to any other hydrogels: sharply swelled at their onset stages, and then nearly approaching a fixed value with time. In order to understand nature of swelling, kinetic modeling was conducted based on a Fickian diffusion law [51, 52].

In general, two types of dynamic swelling modes at initial stages of swelling take place as water molecules intrude into the polymer networks and diffuse: Fickian and non-Fickian behavior. The water intake (S) assumes an exponential relation with time t. The kinetic equation of swelling is presented as follows:

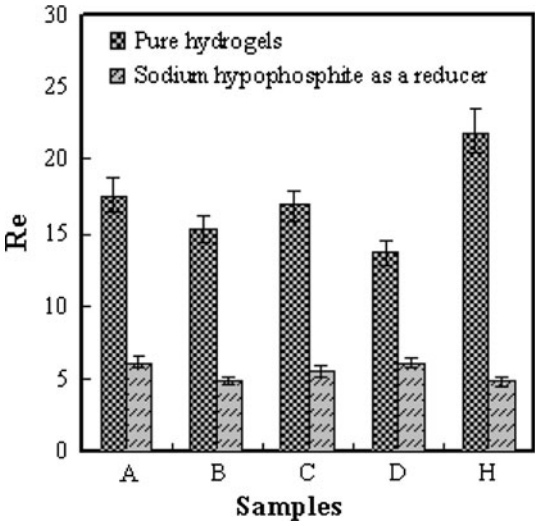

Fig. 6 Equilibrium swelling of different P(AAm-co-NVP)/CS and P(AAm-co-NVP)/CS–Ag hydrogels

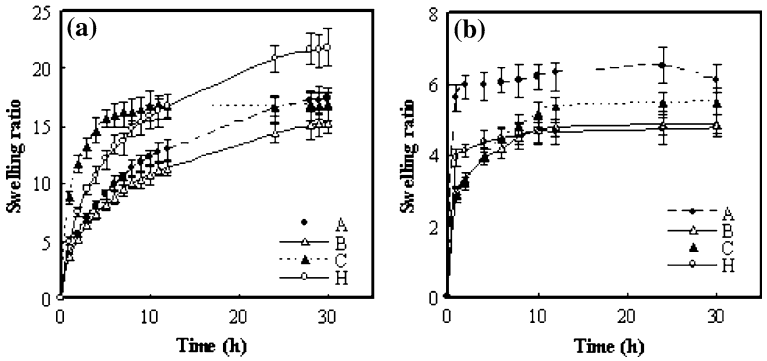

Fig. 7 Dependence of swelling kinetics of (**a**) P(AAm-co-NVP)/CS hydrogels and (**b**) P(AAm-co-NVP)/CS–Ag nanocomposite hydrogels on component ratios

$$\mathrm{F} = S/S_\infty = kt^{\mathrm{n}} \text{ or } \ln(\mathrm{F}) = \ln(S/S_\infty) = \ln(k) + \mathrm{n}\ln(t). \quad (4)$$

The formula is applicable to $S/S_\infty \leq 60\%$, in which S and S_∞ represent the amount of water absorbed by the hydrogel at time t and at an equilibrium state, respectively, k is a characteristic constant of the hydrogel, a parameter which is related to the network structure of polymers, and n is a swelling exponent which reflects solvent diffusion modes or provides information about the mechanism of swelling kinetics inside hydrogels. The constant n and k are calculated from the slopes and intercepts of the graph of $\ln(F)$ against $\ln(t)$ for hydrogels with various component ratios. For $n \leq 0.5$, corresponding to a Fickian diffusion, the rate of diffusion is much slower than the rate of relaxation and for $n = 1$, the diffusion is very fast, contrary to the rate of relaxation and the third case corresponds to an anomalous diffusion with n values between 0.5 and 1.

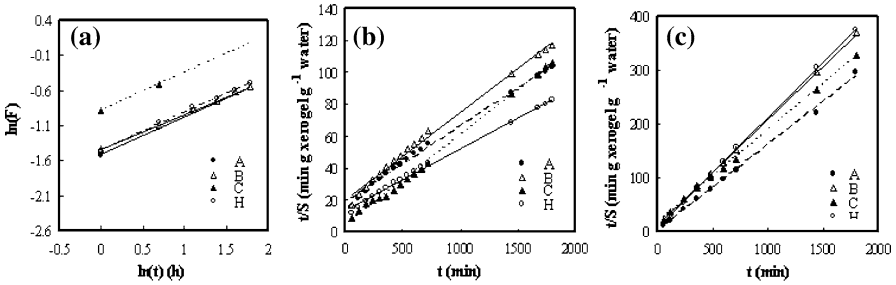

Fig. 8 Linear regression curves of (**a**) P(AAm-co-NVP)/CS hydrogels at the onset stage, (**b**) P(AAm-co-NVP)/CS hydrogels during the whole swelling and (c) t/*S* versus *t* function relations of P(AAm-co-NVP)/CS–Ag nanocomposite hydrogels with a variety of component ratios

Figure 8a can be used to elucidate dependence of $\ln(S_t/S_\infty)$ on $\ln(t)$ for various hydrogel samples with different compositional proportions. After having been fitted, the kinetic parameters k and n as well as the correlation coefficient R^2 obtained are tabulated in Table 3. All the R^2 are greater than 0.99, indicating a small estimated standard error and a high precise linear regression equation. The n values between 0.5 and 1 for all the samples manifest that the diffusion behavior in these hydrogels follows the anomalous diffusion mechanism, and the diffusion is faster than for the Fickian mode. For the examined P(AAm-co-NVP)/CS–Ag systems (Fig. 7b), since the nanocomposite hydrogels are sharply swelled at their onset stages, and S/S_∞ ratios are almost larger than 60% at an interval of 1 h, there is almost no data recoded for fitting. In this case, the rate of polymer chain relaxation is slower than the rate of water diffusion. Therefore, it can be inferred that the initial transport mechanism should approach to non-Fickian mode. After about 1 h, the swelling nearly approaches a fixed value with time. The exponential model (4) cannot be applied in the whole swelling, as stated above. Schott have proposed a second order dynamic model for the extensive swelling of polymers [51].

$$\mathrm{d}S/\mathrm{d}t = k_\mathrm{s}(S_\infty - S)^2 \tag{5}$$

$$t/S = A + Bt, \tag{6}$$

where k_s and S_∞ denote a swelling rate constant and theoretically maximal water volume, respectively; the constant A ($A = 1/k_\mathrm{s}S_\infty^2 = 1/(\mathrm{d}S/\mathrm{d}t)_0$) and B ($B = 1/S_\infty$) are calculated from the slopes and intercepts of the graph of t/S versus t curves for samples with various charge ratios, different initial swelling rate r_0 ($r_0 = 1/A$) values and S_∞. The plots of t/S against t are shown in Fig. 8a and b. After having been fitted, the swelling kinetic equations, k_s, r_0, and S_∞ values of P(AAm-co-NVP)/CS and P(AAm-co-NVP)/CS–Ag hydrogel samples are tabulated in Table 4. Table 4 distinctly shows that these kinetic parameters vary with the component ratios, and the maximal theoretical water volume S_∞ is well in agreement with the experimental values, and the nanocomposite hydrogels have higher swelling rate constants than the control samples.

Table 3 Regression equations and kinetic parameters of P(AAm-co-NVP)/CS semi-IPN hydrogel samples obtained from fitting the experimental data to Ritger–Peppas model

Samples	Initial regression equation	R^2	n	ln(k)
A	$\ln(F) = 0.5314 \ln(t) - 1.5105$	0.9993	0.5314	−1.5105
B	$\ln(F) = 0.5023 \ln(t) - 1.4414$	0.9991	0.5023	−1.4414
C	$\ln(F) = 0.5408 \ln(t) - 0.8905$	1	0.5408	−0.8905
H	$\ln(F) = 0.539 \ln(t) - 1.452$	0.9974	0.5390.	−1.452

Table 4 Extensive swelling kinetic equations, initial swelling rates (r_0), and maximum theoretical water contents (S_∞) of (a). P(AAm-co-NVP)/CS and (b). P(AAm-co-NVP)/CS–Ag hydrogel samples

Systems	Extensive swelling equation*	R^2	S_∞ (g water g^{-1} xerogel)	r_0 (g water g^{-1} xerogel min^{-1})	$K_s \times 10^4$ (g water g^{-1} xerogel min^{-1})
a	$(t/S)_A = 0.0479t + 18.188$	0.9948	20.87683	0.054981	0.041731
	$(t/S)_B = 0.0553t + 19.848$	0.9936	18.08318	0.050383	0.060697
	$(t/S)_C = 0.0565t + 3.9917$	0.9971	17.69912	0.25052	0.012743
	$(t/S)_H = 0.039t + 12.995$	0.9964	25.64103	0.076953	0.019765
b	$(t/S)_A = 0.1593t + 0.9463$	0.9981	6.277464	1.056747	0.024014
	$(t/S)_B = 0.1977t + 11.125$	0.9996	5.058169	0.089888	0.434824
	$(t/S)_C = 0.1728t + 14.994$	0.9989	5.787037	0.066693	0.447718
	$(t/S)_H = 0.2067t + 4.844$	0.9998	4.837929	0.206441	0.206959

**Subscript* A, B, C and H represent the samples in Table 1, respectively

Conclusion

Silver nanoparticles (AgNPs) with different sizes and good dispersibility have been successfully prepared using P(AAm-co-NVP)/CS hydrogel networks as nanoreactor templates. The hydrogel template structure, non-covalent interactions between Ag^+ ions and –OH, $–CONH_2$, $–NH_2$, or –C=O functional groups, steric hindrance as well as reducing ability and charge ratios of the components may have important impact on the nucleation, particle growth, and collision, which is in turn responsible for the fabrication and stabilization of the size- and shape-controllable AgNPs. The AgNPs are stably and uniformly dispersed in P(AAm-co-NVP)/CS networks in the shape of a sphere structure. Thermal analyses further confirm the existence of the AgNPs as well as some chemical interaction within the resulting composites. These results are supported and confirmed by FT-IR, SEM, TEM, and UV–vis findings. The equilibrium swelling and swelling kinetics experiments reveal that the nanocomposite hydrogels possess lower water intake than their original polymer hydrogels. The swelling complies with an anomalous diffusion mechanism at the onset stage and the maximal theoretical water volume is well in agreement with the experimental values. Therefore, the assembly and growth of AgNPs, and the swelling behavior may be controlled and modulated by means of the component

ratios based on the multicomponent templates. The as-prepared P(AAm-co-NVP)/CS–Ag nanocomposites can be expected to find applications in drug carriers, sterilization, or medication materials as novel materials.

Acknowledgment This study was supported by the National Natural Science Foundation of China (grant: 10675078).

References

1. Oh SK, Kim YG, Ye H, Crooks RM (2003) Synthesis, characterization, and surface immobilization of metal nanoparticles encapsulated within bifunctionalized dendrimers. Langmuir 19:10420–10425
2. Mohan YM, Lee K, Premkumar T, Geckeler KE (2007) Hydrogel networks as nanoreactors: a novel approach to silver nanoparticles for antibacterial applications. Polymer 48(1):158–164
3. Akamatsu K, Shinkai H, Ikeda S, Adachi S, Nawafune H, Tomita S (2005) Controlling interparticle spacing among metal nanoparticles through metal-catalyzed decomposition of surrounding polymer matrix. J Am Chem Soc 127:7980–7981
4. Murthy PSK, Mohan YM, Varaprasada K, Sreedhar B, Raju KM (2008) First successful design of semi-IPN hydrogel–silver nanocomposites: a facile approach for antibacterial application. J Colloid Interface Sci 318(2):217–224
5. Guo YG, Hu JS, Liang HP, Wan LJ, Bai CL (2003) Highly dispersed metal nanoparticles porous anodic alumina films prepared by a breathing process of polyacrylamide hydrogel. Chem Mater 15:4332–4336
6. Voronov A, Kohut A, Peukert W (2007) Synthesis of amphiphilic silver nanoparticles in nanoreactors from invertible polyester. Langmuir 23:360–363
7. Shenhar R, Norsten TB, Rotello VM (2005) Polymer-mediated nanoparticle assembly: structural control and applications. Adv Mater 17:657–669
8. He BL, Tan JJ, Liew KY, Liu HF (2004) Synthesis of size controlled Ag nanoparticles. J Mol Catal A 221:121–126
9. Huber K, Witte T, Hollmann J, Keuker-Baumann S (2007) Controlled formation of Ag nanoparticles by means of long-chain sodium polyacrylates in dilute solution. J Am Chem Soc 129:1089–1094
10. Zhu JF, Zhu YJ (2006) Microwave-assisted one-step synthesis of polyacrylamide-metal (M) Ag, Pt, Cu) nanocomposites in ethylene glycol. J Phys Chem B 110:8593–8597
11. Lu DL, Tanaka KI (1997) Au, Cu, Ag, Ni, and Pd particles grown in solution at different electrode potentials. J Phys Chem B 101:4030–4038
12. Li GP, Luo YJ, Tan HM (2004) Preparation of silver nanoparticles using dendrimer as template. Acta Chim Sin 62(12):1158–1161
13. Garcia-Martinez JC, Wilson OM, Scott RWJ, Crooks RM (2006) Extraction of metal nanoparticles from within dendrimer templates. ACS Symp Ser 928:215–229
14. Liu X, Kakkar A (2008) Tailoring silver nanoparticle construction using dendrimer templated silica networks. Nanotechnology 19:245602–245606
15. Vimala K, Sivudu KS, Mohan YM, Sreedhar B, Raju KM (2009) Controlled silver nanoparticles synthesis in semi-hydrogel networks of poly(acrylamide) and carbohydrates: a rational methodology for antibacterial application. Carbohyd Polym 75:463–471
16. Zhang J, Xu S, Kumachev E (2004) Polymer microgels: reactors for semiconductor, metal, and magnetic nanoparticles. J Am Chem Soc 126:7908–7912
17. Kuckling D, Duan VC, Wohlrab SE (2002) Preparation of nanogels with temperature-responsive core and pH-responsive arms by photo-cross-linking. Langmuir 18:4263–4269
18. Kopecek J (2002) Swell gels. Nature 417(6887):388–391
19. Xiang Y, Chen D (2007) Preparation of a novel pH-responsive silver nanoparticle/poly (HEMA–PEGMA–MAA) composite hydrogel. Eur Polym J 43(10):4178–4187
20. Fan X, Huang KL, Liu SQ, Yu JG, Yin LG (2007) Preparation and characteristic of silver nanoparticles by chemical reduction. J Func Mater 6(38):996–1002
21. He R, Qian XF, Yin J, Zhu ZK (2003) Formation of silver dendrites under microwave irradiation. Chem Phys Lett 369(3–4):454–458
22. Schexnailder P, Schmidt G (2009) Nanocomposite polymer hydrogels. Colloid Polym Sci 287:1–11

23. Vinogradov SV (2006) Colloidal microgels in drug delivery applications. Curr Pharm Des 12: 4703–4712
24. Pathak P, Katiyar VK (2007) Cancer research-nanoparticles, nanobiosensors and their use in cancer research. J Nanotechnol 3:1–14
25. Bajpai SK (2006) Analysis of swelling behavior of poly(methacrylamide-co-methacrylic acid) hydrogels and effect of synthesis conditions on water intake. React Funct Polym 66(4):431–440
26. Lin WC, Yu DG, Yang MC (2005) pH-sensitive polyelectrolyte complex gel microspheres composed of chitosan/sodium tripolyphosphate/dextran sulfate: swelling kinetics and drug delivery properties. Colloid Surf B 44(2–3):143–151
27. Rokhade AP, Agnihotri SA, Patil SA (2006) Semi-interpenetrating polymer network microspheres of gelatin and sodium carboxymethyl cellulose for controlled release of ketorolac tromethamine. Carbohyd Polym 65(3):243–252
28. Mohan YM, Vimala K, Thomas V, Varaprasad K, Sreedhar B, Bajpai SK, Raju KM (2010) Controlling of silver nanoparticles structure by hydrogel networks. J Colloid Interface Sci 342:73–82
29. Thomas V, Yallapu MM, Sreedhar B, Bajpai SK (2007) A versatile strategy to fabricate hydrogel–silver nanocomposites and investigation of their antimicrobial activity. J Colloid Interface Sci 315:389–395
30. Tarnavchyk I, Voronov A, Kohut A, Nosova N, Varvarenko S, Samaryk V, Voronov S (2009) Reactive hydrogel networks for the fabrication of metal-polymer nanocomposites. Macromol Rapid Comm 30(18):1564–1569
31. Biswal J, Kumar V, Bhardwaj YK, NK Goel, Dubey KA (2007) Radiation-induced grafting of acrylamide onto guar gum in aqueous medium: Synthesis and characterization of grafted polymer guar-g-acrylamide. Radiat Phys chem 76(10):1624–1630
32. Moshaverinia A, Ansari S, Movasaghi Z, Billington RW, Darr JA, Rehman IU (2008) Modification of conventional glass-ionomer cements with *N*-vinylpyrrolidone containing polyacids, nano-hydroxy and fluoroapatite to improve mechanical properties. Dental Mater 24(10):1381–1390
33. Sun L, Du Y, Chen L, Huang R, Chen X (2004) The synthesis of carboxymethylchitosan hydrogel and the application in drug controlled release systems. Acta Polym Sin 8(2):191–195
34. Moura MR, Aouada FA, Mattoso LHC (2008) Preparation of chitosan nanoparticles using methacrylic acid. J Colloid Interface Sci 321:477–483
35. Yi JZ, Zhang LM (2007) Studies of sodium humate/polyacrylamide/clay hybrid hydrogels: I. Swelling and rheological properties of hydrogels. Eur Polym J 43(8):3215–3221
36. Ng LT, Swami S (2005) IPNs based on chitosan with NVP and NVP/HEMA synthesized through photoinitiator-free photopolymerisation technique for biomedical applications. Carbohyd Polym 60:523–528
37. Dergunov SA, Nam IK, Mun GA, Nurkeeva ZS, Shaikhutdinov EM (2005) Radiation synthesis and characterization of stimuli-sensitive chitosan–polyvinyl pyrrolidone hydrogels. Radiat Phys chem 72:619–623
38. Mane RS, Lee WJ, Pathan HM, Han SH (2005) Nanocrystalline TiO_2-ZnO thin films: fabrication and application to dye-sensitized solar cells. J Phys Chem B 109(51):24254–24259
39. Huang H, Yuan Q, Yang X (2004) Preparation and characterization of metal–chitosan nanocomposites. Colloid Surf B 39(1–2):31–37
40. Patel K, Kapoor S, Dave DP, Mukherjee T (2005) Synthesis of Pt, Pd, Pt/Ag and Ag/Pt nanoparticles by microwave-polyol method. J Chem Sci 117:311–314
41. Kuila BK, Garai A, Nandi AK (2007) Synthesis, optical, and electrical characterization of organically soluble silver nanoparticles and their poly(3-hexylthiophene) nanocomposites: enhanced luminescence property in the nanocomposite thin films. Chem Mater 19(22):5443–5452
42. Long D, Wu G, Chen S (2007) Preparation of oligochitosan stabilized silver nanoparticles by gamma irradiation. Radiat Phys chem 76:1126–1131
43. Chen SP, Wu GZ, Zeng HY (2005) Preparation of high antimicrobial activity thiourea chitosan-Ag^+ complex. Carbohyd Polym 60:33–38
44. Huang HH, Ni XP, Loy GL, Chew CH, Tan KL, Loh FC, Deng JF, Xu GQ (1996) Photochemical formation of silver nanoparticles in poly(N-vinylpyrolidone). Langmuir 12:909–912
45. Wang Y, Li Y, Yang S, Zhang G, An D, Wang C, Yang Q, Chen X, Jing X, Wei Y (2006) A convenient route to polyvinylpyrrolidon/silver nanocomposite by electrospinning. Nanotechnology 17:3304–3307
46. Horák D, Pollert E, Macková H (2008) Properties of magnetic poly(glycidyl methacrylate) and poly(N-isopropylacrylamide) microspheres. J Mater Sci 43:5845–5850

47. Mohan YM, Premkumar T, Lee K, Geckeler KE (2006) Fabrication of silver nanoparticles in hydrogel networks. Macromol Rapid Comm 27:1346–1354
48. Wang XJ, Liu SX, He JH (2006) Fabrication and characteristics of Ag-PVA and Ag-PVA/TiO_2 ultrathin composite films. Photographic Sci Photochem 24(6):421–427
49. Lee WF, Yen SH (2000) Thermoreversible hydrogels. XII. Effect of the polymerization conditions on the swelling behavior of the N-isopropylacrylamide gel. J Appl Polym Sci 78:1604–1611
50. Jin S, Bian F, Liu M, Chen S, Liu H (2009) Swelling mechanism of porous P(VP-*co*-MAA)/PNIPAM semi-IPN hydrogels with various pore sizes prepared by a freeze treatment. Polym Inter 58:142–148
51. Lin ZH, Wu WH, Wang JQ, Jin X (2007) Swelling properties of P(HEMA-co-NEVER) high-strength copolymeric hydrogels. Fine Chem 24:1043–1048
52. Wilder EA, Spontak RJ, Hall CK (2003) The molecular structure and intermolecular interactions of 1, 3:2, 4-dibenzylidene-D-sorbital. Mol Phys 101(19):3017–3027